Research Article | Vol. 13, No. 12 / 1 Dec 2022 / Biomedical Optics Express 6258
Biomedical Optics EXPRESS

Assessing and compensating for the confounding factors in Scheimpflug-based corneal densitometry

MARIA MIAŻDŻYK,[1,*] ALEJANDRA CONSEJO,[2] AND D. ROBERT ISKANDER[1]

[1]Department of Biomedical Engineering, Wroclaw University of Science and Technology, Wybrzeze Wyspianskiego 27, 50-370 Wroclaw, Poland
[2]Department of Applied Physics, University of Zaragoza, Zaragoza, Spain
*maria.miazdzyk@pwr.edu.pl

Abstract: Scheimpflug-based corneal densitometry is a clinically verified method for assessing corneal transparency. Nevertheless, the estimates of corneal densitometry appear to be correlated with age and eye biometry parameters, such as the anterior chamber depth or the pupil size, and that ensues a convoluted conditional estimation problem, where it is difficult to interpret the results. This study aims at devising a methodology for compensating for such confounding factors by using, as a research platform, a commercially available Scheimpflug camera that allows exporting images in a dynamic fashion, allowing averaging the results from multiple acquisitions. Two approaches are considered, one based on appropriately normalizing the line densitometry signal and one based on image histogram equalization. Then, three parameters for describing corneal densitometry are derived including the mean value of backscatter and the scale and shape parameters of the Weibull distribution estimated in regions of interest encompassing parts of corneal stroma. The results show that, unlike the non-normalized measures, the proposed approaches lead to parameters that are not correlated with age nor the eye biometry.

1. Introduction

Scientists have been studying light scattering in the cornea and its transparency for decades [1], but it was not until the early 1980s that quantitative methods were developed to describe this scattering in the human cornea in-vivo [2]. Densitometry is the measurement of optical density and early works with Scheimpflug photographs showed the potential of this technique in examining the properties of light scattering of not only the crystalline lens but also the cornea [3,4]. Commercially available Scheimpflug cameras provided ophthalmologists with tools that allow for widespread study of light scattering in the cornea in everyday clinical practice [5]. Scheimpflug based corneal densitometry was used to show that the average corneal opacity changes after laser surgery [6], and that can act as an early biomarker of subclinical keratoconus [7] or a good indicator of corneal health, for example, during active and healed stages of bacterial keratitis [8]. Nowadays, it became conventional to express corneal densitometry in standardized grayscale units of a digital Scheimpflug image, which in the case of Pentacam HR Scheimpflug device (Oculus Optikgeräte GmbH, Wetzlar, Germany) is calibrated by a proprietary software [9]. So far, this calibration procedure has not been independently verified. As such, corneal densitometry is essentially calculated as the average pixel intensity of the different layers and zones of the cornea. Such a simplified approach to densitometry provides the physician with information, which, unfortunately, depends on a number of factors, including the parameters of the surrounding environment and the biometry of the anterior eye. Additionally, the cornea is not homogeneous with respect to light scattering, and hence the average values may not always provide meaningful information unless they are related to a specific location [5]. Corneal

#473534 https://doi.org/10.1364/BOE.473534
Journal © 2022 Received 18 Aug 2022; revised 17 Oct 2022; accepted 17 Oct 2022; published 7 Nov 2022

Biomedical Optics EXPRESS

densitometry has been shown to be age-dependent [9], but it is easy to show that it is also dependent on the depth of the anterior chamber [10] and pupil size [5]. The biometry parameters also depend on age so investigating the relationships between corneal densitometry and age should, unlike in [10], take into account the confounding biometry factors. In other words, corneal densitometry based on the statistical characteristics of an unprocessed Scheimpflug image is a convoluted problem where interpretive problems may occur.

Early works on Scheimpflug-photography-based anterior segment densitometry identified several standardization techniques for compensating for some of the confounding factors [11,12]. From those works, setting the peak height of the second main corneal shoulder in the line densitometry signal to a predetermined value appeared to give the best results [5], reducing the overall effect of some of confounding factors such as the parameters of photographic film. Here, the shoulder is understood as the inflection point in the signal corresponding to the transition between epithelium and stroma, whereas the signal itself represents a single column/row in a densitometry image. However, to the best of the authors' knowledge, no freely available information exists on the standardization methods implemented in the Pentacam HR Scheimpflug device.

Corneal Visualization Scheimpflug Technology (Corvis ST, Oculus Optikgeräte GmbH, Wetzlar, Germany) is yet another Scheimpflug-principle-based device that, although does not display corneal densitometry values, can be used to study corneal backscatter properties as it allows exporting images in a dynamic fashion [13], allowing multiple acquisitions and facilitating better statistical characterisation of the corneal backscatter parameters than in the case of static acquisitions. The purpose of this study was to use Corvis ST as a research platform to examine the influence of age and anterior eye biometry on the parameters of corneal backscatter in Scheimpflug imaging and devise a methodology for compensating for that influence.

2. Materials and methods

2.1. Preliminaries

Scheimpflug images of the cornea of younger subjects are visibly different to those of older subjects, as shown in Fig. 1. The main difference between images of older subjects in comparison to those of the young subjects is a stronger appearance of iris backscatter caused by the shallower anterior chamber depth (ACD, here defined as the distance between anterior corneal surface and anterior lens surface). Additionally, in some images of older subjects, the outline of the pupil size (PUP) is apparent (see Fig. 1(A), (B), (D) and (F)).

As it will be shown later, after image segmentation the statistical characteristics of corneal backscatter are correlated with the average pixel intensity of the background segment, in the following denoted by $\overline{\mathrm{BCG}}$, situated just below the corneal segment, and this correlation is prevalent in images of both young and old subjects. Hence, this first-glance observation suggests an influence of the anterior eye biometry on the corneal backscatter. Taking the simple measure of an average pixel intensity in a given corneal region may produce differences between the estimates for the young subjects in comparison to those for older subjects, but that difference may be simply due to the anterior eye geometry but not to the corneal tissue transparencies themselves. Hence, when corneal densitometry measurements are considered, the challenge is to process such corneal Scheimpflug images in a way that reduces the effect of confounding factors related to the anterior eye biometry.

2.2. Data

The study includes retrospective data obtained from Corvis ST air-puff tonometer and IOLMaster 700 biometer (Carl Zeiss Meditec AG, Jena, Germany). Two groups of subjects were considered: a group of 141 young subjects of age $\leq$ 30 years and a group of 73 older subjects of age $\geq$ 50

Biomedical Optics EXPRESS

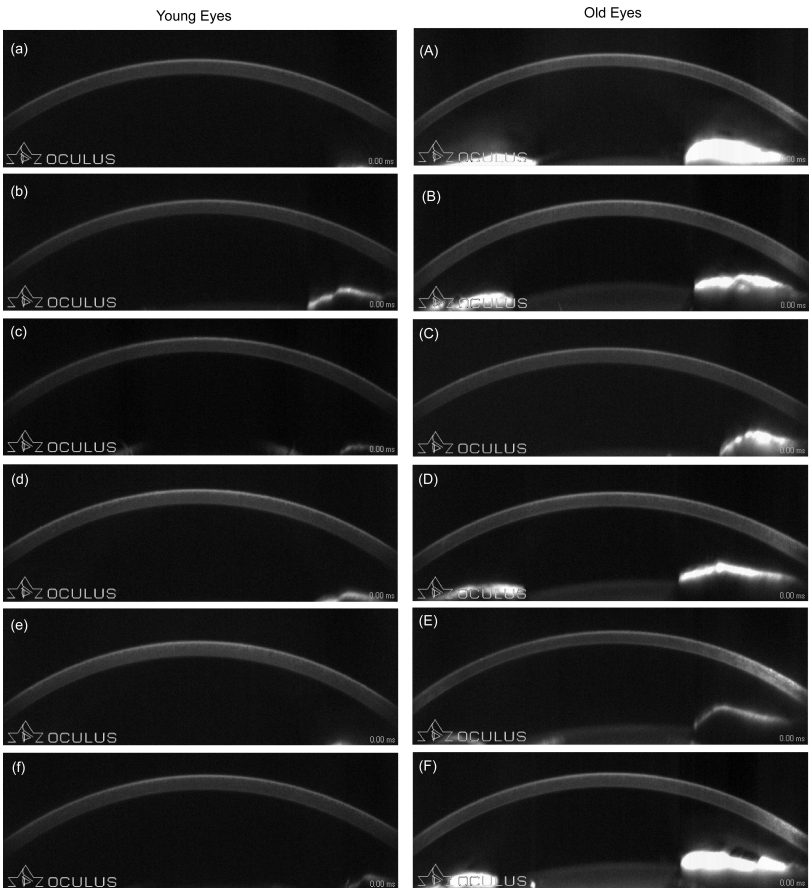

Fig. 1. Illustrative examples of Scheimpflug-principle-based imaging of cornea for younger subjects (left column) and for older subjects (right column), acquired with Corvis ST.

years. Throughout the paper, those two groups of subjects are denoted simply as group Y and group O, respectively. The rationale behind this particular age distinction is to provide two cohorts of subjects with distinct changes in anterior eye biometry as it is known that ACD and PUP are reducing with age [14,15] whereas the central corneal thickness (thickness measured in the apex of the cornea, from now CCT) may not [16]. Exclusion criteria included any previous history of cornea or intraocular surgery, any pathology in corneal scarring such as dystrophies and trauma. Also, any ectatic condition such as keratoconus was excluded. Following [17], one randomly chosen eye of each subject was considered.

For each subject, Corvis ST data includes a sequence of 140 Scheimpflug images showing the corneal dynamic response to an air-puff. From each such sequence, the first 10 frames and the last 10 frames, where the cornea was in its convex state (i.e., before being applanated and after returning to its initial state), were taken for the analysis. Data was reviewed and tested to ascertain that no statistically significant differences exist between the initial eye position and that after the air-puff. Gray scale images were of size 576×200 pixels with the estimated resolution of 14.8 μm/pixel horizontally and 24.0 μm/pixel vertically.

IOLMaster 700 data included a set of biometry parameters, from which ACD, PUP, and CCT were recorded. Subject's age (in years) was also noted. Table 1 shows the considered population mean values ($\pm$ one standard deviation) and ranges for age and biometry parameters.

Biomedical Optics EXPRESS

The differences in ACD and PUP between Y and O group are statistically significant, whereas the difference in CCT is not, as desired.

Table 1. Mean ± one standard deviation and range [.,.] of age and eye biometry parameters for three groups including all subjects (Y & O), only young (Y), and only old (O) subjects. The last column shows the results of the two sample *t*-test.

	Y & O	**Y**	**O**	**Y** vs. **O**
	(n = 214)	(n = 141)	(n = 73)	p
Age [years]	36.7 ± 18.6	23.6 ± 2.3	61.7 ± 6.3	–
	[20, 75]	[20, 30]	[50, 75]	
ACD [mm]	3.37 ± 0.40	3.56 ± 0.29	3.00 ± 0.31	<0.001
	[2.31, 4.25]	[2.64, 4.25]	[2.31, 3.73]	
PUP [mm]	4.8 ± 1.2	5.3 ± 1.0	3.7 ± 0.6	<0.001
	[2.6, 8.1]	[2.8, 8.1]	[2.6, 5.4]	
CCT [μm]	556 ± 32	558 ± 30	551 ± 34	0.059
	[468, 640]	[468, 640]	[474, 623]	

Because densitometry parameters correlate with age [9], whereas the biometry in this study appears to confound the results of corneal backscatter assessment, it is important first to establish how the biometry parameters are correlated with age for the considered cohort of subjects. Table 2 shows the Pearson's correlation coefficients and the corresponding p-values for the three considered biometry parameters. Figure 2 shows the corresponding general trends in the biometry parameters with age. Those preliminary results closely correspond to those obtained for other populations [14], indicating that the selected cohort of subjects is adequate for this study.

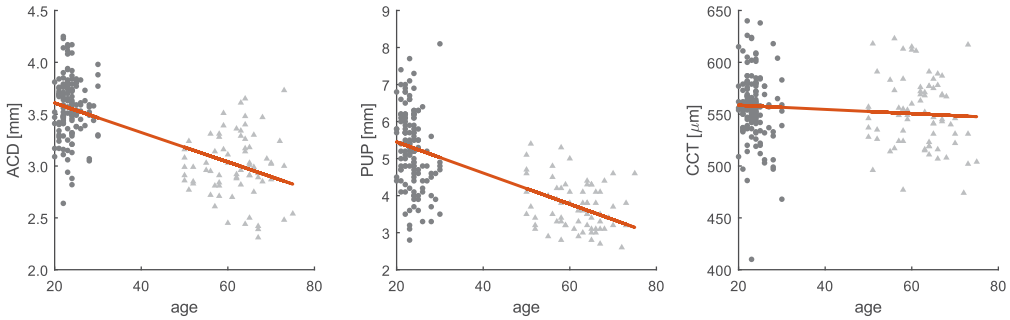

Fig. 2. Scatter plots of biometry parameters ACD, PUP, and CCT as functions of age, for both young (dark gray circles) and old subjects (light gray triangles). Orange lines show the general trends of these parameters with age (see also Table 2)

2.3. Corneal densitometry parameters

Three parameters describing the statistical properties of the corneal backscatter were considered: the mean value (referred to simply as densitometry, d, in the remaining of this work) and the two parameters (scale and shape) of the Weibull distribution with probability density function given by

$$f_X(x;\alpha,\beta) = \frac{\beta}{\alpha}\left(\frac{x}{\alpha}\right)^{\beta-1} e^{-(x/\alpha)^{\beta}} \quad \text{for} \quad x \geq 0, \tag{1}$$

where α>0 is the scale parameter, β>0 is the shape parameter and x denotes the values of image pixel intensity in a specified region of interest (ROI) encompassing corneal stroma (see Section

Biomedical Optics EXPRESS

Table 2. Pearson's correlation coefficients, *r*, and the corresponding *p*-values for correlation of biometry parameters (ACD, PUP, CCT) with age, for three groups including all subjects (Y & O), only young (Y), and only old (O). Bold font indicates significant non-zero correlations at 5% level of significance and 80% power for the given sample sizes, *n*.

		Y & O (n = 214)	Y (n = 141)	O (n = 73)
ACD	r	**−0.663**	−0.006	−0.022
	p	**<0.001**	0.947	0.857
PUP	r	**−0.657**	**−0.284**	−0.277
	p	**<0.001**	**0.001**	0.018
CCT	r	−0.112	−0.137	−0.134
	p	0.101	0.106	0.258

2.5). The parameters α and β are estimated using the methods of maximum likelihood. For Scheimpflug images, the corneal densitometry parameter estimators $\{\hat{d}, \hat{\alpha}, \hat{\beta}\}$ showed statistically significant correlations with the image background, necessitating some processing of those images (see Section 2.6) after which these correlations were substantially reduced.

2.4. Pupil size

The pupil size, PUP, measured with IOLMaster 700 with a frontal camera does not necessarily correspond to that observed in Scheimpflug images recorded with Corvis ST, despite all measurements being performed in the same room in mesopic lighting conditions. Hence, it was of interest whether for a subgroup of Scheimpflug images, where the outline of the pupil was visible, the manually extracted pupil size (i.e., the distance between iris edges) would correspond to that measured with IOLMaster 700. Out of the total number of subjects, 49 subjects were identified to have such image characteristics (only the first frame was considered in each sequence). The measurement was performed with digital calipers. Correlation between PUP measured with IOLMaster 700 to that extracted from Scheimpflug images of Corvis ST was strong ($r = 0.788$) and highly statistically significant ($p \ll 0.001$, see Fig. 3). On average, the PUP measured with IOLMaster 700 was 9% larger than that extracted from Corvis ST, which well agrees with the theoretical result [18].

2.5. Image segmentation

The image segmentation algorithm, described earlier in [19], was extended to account for three distinct corneal regions: temporal (T), central (C), and nasal (N). Additionally, the algorithm was improved to be more robust for images of older eyes. That included mostly adjusting the parameters of the Canny's edge detection algorithm. Images of the left eyes were flipped along the vertical axis to correspond to those of the right eyes. ROI size (see mask in Fig. 4) was determined empirically with the following criteria: maximize the ROI width and at the same time avoid the influence of boundary effects (e.g., the light backscatter near the image periphery). The central ROI covers about 1.8 mm of the horizontal corneal section. Symmetrically situated temporal and nasal ROI cover the corneal diameter section at a range from about 2 mm to 4 mm. Peripheral parts of the cornea were not considered. That is, the left and right margins were determined empirically to about 1.5 mm. Because distinguishing particular layers (i.e., epithelium, Bowman's layer, Descemet's membrane, and endothelium) is difficult in those low resolution Scheimpflug images, only the stroma and endothelium, whose scattering properties are not that different from those of stroma, were included in the analysis. Therefore, a margin of 120 μm (5 pixels) from the corneal anterior surface was set. Additionally, because the corneal

Biomedical Optics EXPRESS

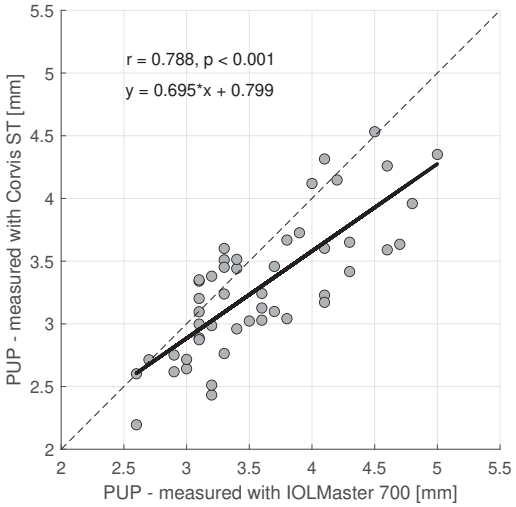

Fig. 3. The relationship between pupil size (PUP) measured with IOLMaster 700 to that extracted from Scheimpflug images of Corvis ST.

densitometry parameters were first found to correlate also with CCT, the depth of the ROI was fixed to 13 pixels, to fit to the thinnest cornea in the considered cohort of subjects.

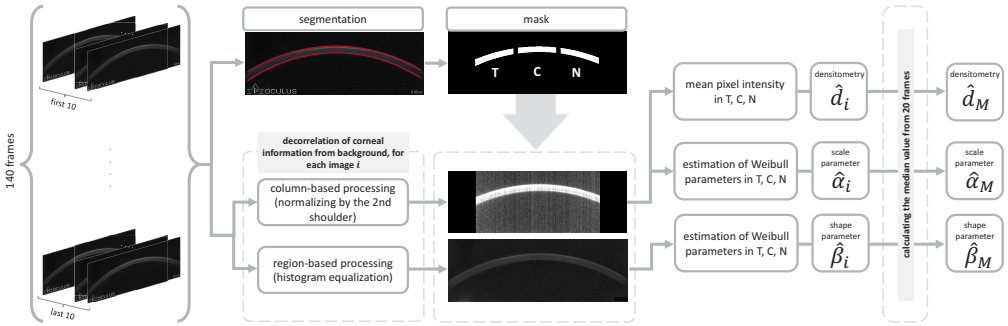

Fig. 4. Schematic of the final methodology developed for compensating corneal densitometry parameters for confounding factors related to age and eye biometry.

One may debate whether the size of the eye affects the predefined T, C, and N ROIs. Simplifying the measured corneal surface as a circular segment with the smallest and largest radius of 7.2 mm and 8.5 mm, respectively, the difference in the arc length for those two segments is less that 0.2 mm. That is why, in this work the lateral positions of the ROIs are fixed.

2.6. Image processing

The schematic overview of the final methodology developed for compensating corneal densitometry parameters for confounding factors related to anterior eye geometry is shown in Fig. 4. There have been a several dozen attempts (see Section 4.) before arising at this final stage. The company logo placed in the south-west corner of the image was first removed by replacing its pixels by a set of Gaussian random variables with mean and standard deviation corresponding to the sample mean and sample standard deviation of the logo surroundings.

For each of the 20 (i.e., the first 10 and the last 10) images of the sequences recorded for each subject, three parallel processing steps were first considered: image segmentation as described in

Biomedical Optics EXPRESS

Section 2.5, column-based processing of an image, in which each pixel intensity profile (i.e., image column) was normalized by its value at the second corneal shoulder (i.e., by the value at which the slope at the shoulder is greatest), and region-based processing involving adaptive histogram equalization. As shown in Fig. 5, the first corneal shoulder in the central densitometry profile corresponds to the air/epithelium interface, the second corneal shoulder to the epithelium/stroma interface whereas the third shoulder corresponds to endothelium/anterior chamber interface. The exact position of a given corneal shoulder was calculated by first smoothing the pixel intensity profile using the Savitzky-Golay infinite impulse response filter of polynomial order of 3 and the window size of 11, then calculating the first derivative of such smoothed profile and, finally, identifying where it achieves local extrema within the segmented earlier corneal sector. From the three considered shoulders, only the normalization by the second corneal shoulder achieved the desired decorrelation results.

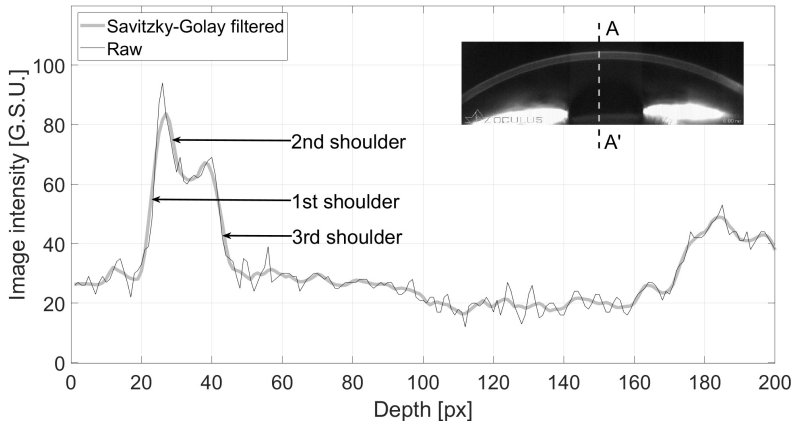

Fig. 5. Illustrative central pixel intensity profile (AA') for an image of an older subject with three distinct corneal shoulders indicated by arrows. Only normalization by the 2nd shoulder (i.e., by the value of the greatest slope of the pixel intensity profile at this shoulder), provided satisfactory decorrelation results. G.S.U. – gray scale units.

The adaptive histogram equalization was performed by dividing the image into 64 rectangular contextual regions with the desired histogram shape governed by a Rayleigh distribution with a scale parameter $\sigma = 0.2$. All the parameters of histogram equalization were determined experimentally in order to minimize in images the inherent correlation between densitometry parameters $\{d, \alpha, \beta\}$ and the mean of the background lying just below the considered ROI.

The output of the above-described algorithms consists of three components: corneal regions of interest (mask), corresponding to temporal (T), central (C), and nasal (N) corneal regions, a column-processed image and a region-processed image, for which adaptive histogram equalization was applied.

In the next stage of the proposed methodology, the parameters d and α are estimated in each considered corneal region from the column-based processed image whereas the parameter β from the region-based processed image. This distinction was necessary (see Table 3 in Section 3 below) because a single image processing procedure, for which both estimates of the scale and shape parameters of the Weibull distribution would decorrelate from the mean background could not be currently devised. In the final stage of the procedure, median values (across the 20 input images) were calculated leading to a set of estimators $\{\hat{d}_M, \hat{\alpha}_M, \hat{\beta}_M\}$.

Biomedical Optics EXPRESS

Table 3. Indication of decorrelation (✓) or statistically significant correlation (×) between corneal densitometry parameters $\{d_M, \alpha_M, \beta_M\}$ and image background $\overline{\mathrm{BCG}}_M$ for the group of all subjects. Orange color denotes the decorrelation results for the final methodology from Fig. 4.

Decorrelation method		Y&O		
		T	C	N
none (unprocessed images)	$\hat{d}_M$	×	×	×
	$\hat{\alpha}_M$	×	×	×
	$\hat{\beta}_M$	×	×	×
normalize (2nd shoulder)	$\hat{d}_M$	✓	✓	✓
	$\hat{\alpha}_M$	✓	✓	×
	$\hat{\beta}_M$	×	×	×
histogram equalization	$\hat{d}_M$	×	×	×
	$\hat{\alpha}_M$	×	×	×
	$\hat{\beta}_M$	✓	✓	✓

2.7. Statistical analyses

All the variables were tested for the null hypothesis of Gaussian distribution using the Jarque-Bera test. The level of significance was set to 5%. The pair-wise relationships between the considered biometry and densitometry parameters as well as between the latter and the mean image background were assessed with Pearson correlation coefficient. Correlations were deemed statistically significantly different from the null correlation of zero at 5% level of significance and 80% power for the given sample sizes, resulting in three correlation threshold values of $r \geq 0.191$, $r \geq 0.234$, and $r \geq 0.323$ for Y&O ($n = 214$), Y ($n = 141$), and O ($n = 73$) group, respectively. Hence, the correlation was classified as statistically significant if p-value was smaller than 0.05 and, at the same time, the Pearson correlation coefficient exceeded the threshold value.

3. Results

Before going into the detailed analysis, it is convenient to provide a general overview of what were the correlations of the corneal backscatter parameters ($\{\hat{d}_M, \hat{\alpha}_M, \hat{\beta}_M\}$) with the image background ($\overline{\mathrm{BCG}}_M$) before and after application of a decorrelation method. Table 3 depicts those correlations, where ✓ denotes successful decorrelation and × denotes statistically significant correlation (unsuccesful). Figure 6 depicts a summary of correlations of densitometry parameters with age and biometry parameters before and after image normalization. Examining the details, for unprocessed images (see Table 4 for full correlation results), the densitometry parameter estimators $\hat{d}_M$ and $\hat{\alpha}_M$ can be considered to be unrelated to the image background only for the group of older subjects, whereas the parameter estimator $\hat{\beta}_M$ is correlated with $\overline{\mathrm{BCG}}_M$ for all considered groups. Different types of image normalization, whether when using column-based or region-based processing, affect those correlations. It becomes apparent (highlighted by orange font in Table 3) that column-based normalization by the 2nd corneal shoulder results in decorrelation of parameter estimators $\hat{d}_M$ and $\hat{\alpha}_M$ (except for Y&O nasal) from the background whereas the region-based normalization decorrelates $\hat{\beta}_M$ from $\overline{\mathrm{BCG}}_M$ (see Table 5 and Table 6 for full correlation results, respectively).

It is also evident now, as it was hinted earlier, that for unprocessed images, when considering all subjects, the mean background in Scheimpflug images is statistically significantly correlated with age, ACD and PUP – a result that prompted the necessity for processing such images. For column-based processing (see Table 5), the densitometry parameter estimator $\hat{d}_M$ does not statistically significantly correlate with either age or the biometry parameters whereas its distributional

Biomedical Optics EXPRESS

Table 4. Pearson correlation coefficients *r* and corresponding *p*-values for the three considered densitometry parameter estimators $\{\hat{d}_M, \hat{\alpha}_M, \hat{\beta}_M\}$, age, eye biometry parameters (ACD, PUP, CCT), and the mean image background $\overline{\text{BCG}}_M$ for unprocessed images. Bold font indicates significant non-zero correlations at 5% level of significance and 80% power.

		Y&O			Y			O		
		T	C	N	T	C	N	T	C	N
$\hat{d}_M$										
AGE	*r*	**0.322**	**0.265**	**0.499**	**0.310**	**0.303**	**0.306**	0.226	0.204	**0.341**
	p	**<0.001**	**<0.001**	**<0.001**	**<0.001**	**<0.001**	**<0.001**	0.055	0.084	**0.003**
ACD	*r*	**−0.251**	−0.121	**−0.436**	−0.178	−0.129	−0.150	0.071	0.310	−0.277
	p	**<0.001**	0.077	**<0.001**	0.034	0.127	0.077	0.548	0.008	0.018
PUP	*r*	**−0.273**	**−0.266**	**−0.374**	−0.175	−0.189	−0.137	−0.005	−0.122	−0.205
	p	**<0.001**	**<0.001**	**<0.001**	0.038	0.024	0.106	0.966	0.304	0.083
CCT	*r*	0.077	0.022	0.005	0.133	0.101	0.070	0.059	−0.050	0.043
	p	0.261	0.749	0.941	0.117	0.232	0.411	0.621	0.673	0.719
$\hat{\alpha}_M$										
AGE	*r*	**0.302**	**0.239**	**0.480**	**0.316**	**0.304**	**0.308**	0.211	0.196	**0.334**
	p	**<0.001**	**<0.001**	**<0.001**	**<0.001**	**<0.001**	**<0.001**	0.073	0.097	**0.004**
ACD	*r*	**−0.232**	−0.109	**−0.426**	−0.167	−0.123	−0.149	0.074	0.287	−0.285
	p	**0.001**	0.111	**<0.001**	0.048	0.145	0.077	0.535	0.014	0.015
PUP	*r*	**−0.255**	**−0.241**	**−0.361**	−0.170	−0.178	−0.137	0.014	−0.101	−0.203
	p	**<0.001**	**<0.001**	**<0.001**	0.044	0.034	0.104	0.906	0.397	0.085
CCT	*r*	0.084	0.035	0.009	0.132	0.104	0.067	0.072	−0.028	0.050
	p	0.224	0.607	0.896	0.118	0.221	0.430	0.546	0.813	0.675
$\hat{\beta}_M$										
AGE	*r*	**0.422**	**0.438**	**0.247**	−0.106	−0.076	−0.097	0.118	0.189	−0.008
	p	**<0.001**	**<0.001**	**<0.001**	0.211	0.372	0.251	0.320	0.110	0.944
ACD	*r*	**−0.332**	−0.185	−0.088	−0.191	−0.026	0.013	0.047	**0.332**	0.217
	p	**<0.001**	0.007	0.199	0.023	0.760	0.883	0.694	**0.004**	0.065
PUP	*r*	**−0.369**	**−0.405**	−0.177	−0.123	−0.163	0.023	−0.237	**−0.323**	−0.072
	p	**<0.001**	**<0.001**	0.010	0.147	0.054	0.784	0.044	**0.005**	0.544
CCT	*r*	−0.186	**−0.197**	−0.155	−0.081	−0.076	−0.050	−0.264	−0.287	−0.222
	p	0.006	**0.004**	0.023	0.342	0.368	0.553	0.024	0.014	0.058
$\overline{\text{BCG}}_M$										
AGE	*r*	**0.568**	**0.537**	**0.623**	**0.239**	0.195	**0.244**	0.078	0.159	0.090
	p	**<0.001**	**<0.001**	**<0.001**	**0.004**	0.020	**0.004**	0.513	0.179	0.450
ACD	*r*	**−0.557**	**−0.612**	**−0.530**	**−0.354**	**−0.454**	**−0.331**	−0.287	**−0.487**	−0.159
	p	**<0.001**	**<0.001**	**<0.001**	**<0.001**	**<0.001**	**<0.001**	0.014	**<0.001**	0.180
PUP	*r*	**−0.517**	**−0.368**	**−0.501**	**−0.252**	−0.084	−0.169	**−0.389**	−0.073	−0.313
	p	**<0.001**	**<0.001**	**<0.001**	**0.003**	0.323	0.045	**0.001**	0.538	0.007
CCT	*r*	−0.049	−0.003	−0.018	−0.047	0.097	−0.063	0.034	0.035	0.120
	p	0.473	0.966	0.796	0.584	0.253	0.460	0.773	0.770	0.312
$\hat{d}_M$	*r*	**0.257**	**0.234**	**0.396**	**0.392**	**0.339**	0.164	−0.056	0.067	0.175
	p	**<0.001**	**0.001**	**<0.001**	**<0.001**	**<0.001**	0.052	0.635	0.573	0.138
$\hat{\alpha}_M$	*r*	**0.231**	**0.218**	**0.379**	**0.371**	**0.314**	0.155	−0.079	0.071	0.167
	p	**0.001**	**0.001**	**<0.001**	**<0.001**	**<0.001**	0.067	0.509	0.550	0.159
$\hat{\beta}_M$	*r*	**0.520**	**0.289**	**0.389**	**0.397**	**0.299**	0.178	**0.375**	0.028	**0.330**
	p	**<0.001**	**<0.001**	**<0.001**	**<0.001**	**<0.001**	0.034	**0.001**	0.812	**0.004**

Biomedical Optics EXPRESS

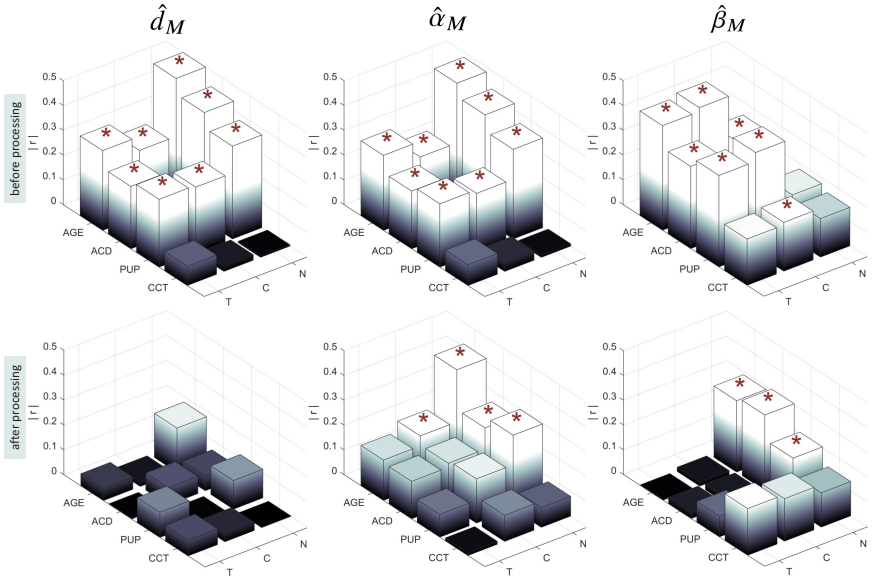

Fig. 6. A pictorial summary of correlations (absolute values) of Y&O densitometry parameters $\{\hat{d}_M, \hat{\alpha}_M, \hat{\beta}_M\}$ with age and biometry parameters (ACD, PUP, CCT) before (top) and after (bottom) image processing (see Fig. 4). Asterisks denote statistically significant correlations.

equivalent, the scale parameter estimator $\hat{\alpha}_M$, shows statistically significant correlation with age in the central corneal region despite being decorrelated from the mean background. The inability to decorrelate $\hat{\alpha}_M$ from the background in the nasal side can be attributed to the potential asymmetry between the nasal and temporal regions of a Scheimpflug image. Further, for region-based processing (see Table 6), the shape parameter estimator $\hat{\beta}_M$, although successfully being decorrelated from the mean background, shows statistically significant correlation with age, ACD and PUP for the nasal side. Again, potential asymmetry between the nasal and temporal regions of a Scheimpflug image may contribute to these results.

4. Discussion

Aging of the eye is not a linear process and the same is also valid for the cornea. In general, one expects some corneal parameters of a young person to be different to those of the cornea of an older person. Also, for the older group, it is difficult to separate specific changes related to age from changes that have been modified by the environmental or genetic factors [20]. When examining changes in selected parameters of the cornea with age, one should take into account the fact that in the younger group of subjects, the variability in a given parameter may be small enough to exhibit its high correlation with age. On the other hand, for older subjects such a parameter may have high variability, which in turn would result in insignificant correlation of it with age. Also when examining both groups together, arriving at statistically significant correlations of corneal parameters with age (or with ACD and PUP) may be governed by the existence of two separate clusters. That is why, in this study, two age-groups of subjects were considered and examined separately and also, for comparison, as a one group (Y&O).

Corneal densitometry acquired from Scheimpflug images of the anterior eye segment is a corroborated technique used for assessing corneal transparency in a clinical ophthalmology practice [8,21,22]. It is useful for assessing the effect of treatment [23–25] (so-called *before* and *after* measurements), as in such cases the influence of the biometry parameters or the patient's

Biomedical Optics EXPRESS

Table 5. Pearson correlation coefficients *r* and corresponding *p*-values for the parameter estimators $\{\hat{d}_M, \hat{\alpha}_M\}$, age, eye biometry parameters (ACD, PUP, CCT), and the mean image background $\overline{\text{BCG}}_M$ for column-based processed images (normalization with the 2nd corneal shoulder). Bold font indicates significant non-zero correlations at 5% level of significance and 80% power.

		Y&O (n = 214)			**Y** (n = 141)			**O** (n = 73)		
		T	C	N	T	C	N	T	C	N
$\hat{d}_M$										
AGE	*r*	0.049	−0.018	−0.177	0.002	−0.016	0.012	0.067	−0.003	−0.183
	p	0.480	0.794	0.009	0.984	0.853	0.892	0.573	0.981	0.121
ACD	*r*	0.002	0.069	0.059	−0.028	0.002	−0.097	0.144	0.174	−0.020
	p	0.973	0.316	0.387	0.743	0.984	0.250	0.223	0.142	0.868
PUP	*r*	−0.101	0.003	0.115	−0.081	0.027	0.014	−0.156	−0.089	0.034
	p	0.140	0.963	0.094	0.340	0.752	0.873	0.188	0.456	0.777
CCT	*r*	−0.063	0.032	−0.001	0.071	0.070	0.006	−0.261	−0.017	−0.047
	p	0.357	0.637	0.989	0.405	0.406	0.948	0.026	0.887	0.695
$\hat{\alpha}_M$										
AGE	*r*	−0.163	**−0.203**	**−0.413**	0.009	0.024	0.024	−0.006	−0.081	**−0.365**
	p	0.017	**0.003**	**<0.001**	0.920	0.780	0.779	0.959	0.497	**0.002**
ACD	*r*	0.151	0.167	**0.253**	0.049	0.033	−0.052	0.057	0.060	0.060
	p	0.027	0.015	**<0.001**	0.562	0.695	0.542	0.631	0.613	0.614
PUP	*r*	0.092	0.178	**0.297**	−0.010	0.089	0.048	−0.044	0.037	0.171
	p	0.182	0.009	**<0.001**	0.906	0.294	0.571	0.714	0.757	0.149
CCT	*r*	0.012	0.105	0.079	0.099	0.082	0.038	−0.160	0.103	0.068
	p	0.863	0.124	0.248	0.244	0.333	0.656	0.177	0.387	0.565
		Y&O			**Y**			**O**		
		T	C	N	T	C	N	T	C	N
$\overline{\text{BCG}}_M$										
$\hat{d}_M$	*r*	0.097	0.037	−0.063	−0.064	−0.022	0.117	0.199	0.090	0.017
	p	0.158	0.587	0.363	0.447	0.795	0.165	0.091	0.451	0.887
$\hat{\alpha}_M$	*r*	−0.114	−0.091	**−0.325**	−0.177	−0.151	0.029	0.073	0.088	−0.216
	p	0.097	0.185	**<0.001**	0.035	0.075	0.730	0.538	0.459	0.066

age is not considered to confound the differential results. However, when assessing the effect of treatment that may influence anterior eye biometry, for example, implantation of intrastromal corneal ring segment [26], caution should be exercised when interpreting such results. Also, when studying the corneal backscatter properties for populations, particularly subjects with different age, both the age and the anterior eye biometry seem to confound the results of currently established corneal densitometry [5,10]. The influence of age on corneal tissue is widely reported in the literature. To mention just a few, the studies of Niederer et al. [27] showed a decrease in stromal keratocyte and endothelial cell density due to corneal ageing. Daxer et al. [28] indicated that stromal collagen fiber diameter and axial period increase with age, while Sharma et al. [29] documented decrease of small nerve fiber density in epithelium and Bowman's layer. Corneal speckle in optical coherence tomography studies likewise showed statistically significant differences between age groups in the stroma [30]. Also, mean corneal backscatter received from confocal microscopy in vivo, which seems to be less influenced by eye biometry than Scheimpflug

Biomedical Optics EXPRESS

Table 6. Pearson correlation coefficients *r* and corresponding *p*-values for the parameter estimator $\hat{\beta}_M$, age, eye biometry parameters (ACD, PUP, CCT), and the mean image background $\overline{\text{BCG}}$ for region-based processed images (histogram equalization). Bold font indicates significant non-zero correlations at 5% level of significance and 80% power.

		Y&O (n = 214)			**Y** (n = 141)			**O** (n = 73)		
		T	C	N	T	C	N	T	C	N
$\hat{\beta}_M$										
AGE	r	−0.003	−0.017	**−0.288**	−0.090	−0.230	−0.168	−0.138	−0.004	−0.150
	p	0.968	0.805	**<0.001**	0.290	0.006	0.047	0.244	0.973	0.207
ACD	r	−0.026	0.022	**0.304**	−0.028	−0.015	0.096	0.004	0.117	0.273
	p	0.705	0.747	**<0.001**	0.746	0.864	0.257	0.976	0.323	0.019
PUP	r	−0.084	−0.033	**0.204**	−0.119	−0.075	0.071	−0.051	0.062	0.037
	p	0.221	0.632	**0.003**	0.158	0.376	0.405	0.670	0.600	0.755
CCT	r	−0.188	−0.171	−0.138	−0.178	−0.119	−0.121	−0.205	−0.269	−0.227
	p	0.006	0.012	0.043	0.035	0.158	0.151	0.082	0.022	0.053
		Y&O			**Y**			**O**		
		T	C	N	T	C	N	T	C	N
$\overline{\text{BCG}}_M$										
$\hat{\beta}_M$	r	0.174	−0.063	−0.062	0.228	0.035	−0.034	0.184	−0.161	0.191
	p	0.011	0.361	0.370	0.006	0.679	0.692	0.119	0.174	0.106

images, indicated differences between age groups in the anterior stroma [31]. Despite other imaging techniques indicating changes in corneal stroma microstructure with aging, densitometry results of this study, which are compensated for confounding factors, remain correlated with age only in the nasal ROI, for $\hat{\alpha}_M, \hat{\beta}_M$ parameters and in the central, for $\hat{\alpha}_M$, whereas $\hat{d}_M$ seems to be fully uncorrelated with age and biometry. Nevertheless, no evident correlation with age in the assessed here corneal densitometry parameters does not preclude microstructure changes, but rather indicates that the applied imaging method is not suitable for the analysis of tissue ageing. Particularly, the resolution of analyzed here Scheimpflug images is insufficient to assess any potential corneal tissue reorganization based on its backscatter. To assess the efficacy of this technique, the analogous analysis on higher resolution Scheimpflug images should be performed. Although in the literature there are works showing dependence of age on corneal densitometry [9,13], it is important to consider which part of such dependence is determined by confounding factors, e.g., stemming from the relationship between age and biometry, and which part originates from corneal microstructure ageing.

Since there is no publicly available information on the way corneal densitometry is calculated and the *standardized grayscale units* used in the current commercial instrumentation to express the estimates of that densitometry are nowhere defined, it is difficult to assess the value of a continually increasing number of studies on the subject as the results, in most of those studies, seem to be confounded by both anterior eye biometry and subject's age. Therefore, in this work, using two cohorts of young and old subjects, it was aimed to first assess that potential effect of confounding factors and then devise the techniques for compensating them. The topic is not new as the need for compensating for such factors was already identified in the late eighties when Scheimpflug photography was first utilized for assessing properties of cornea (see the review of Wegener et al., 2009 [5]) but those early developments seem to have stalled. The current study fills the apparent gap in research related to Scheimpflug based corneal densitometry.

Biomedical Optics EXPRESS

It needs to be acknowledged that the techniques for standardizing Scheimpflug images have been verified only for the case of Corvis ST and this is a limitation. Nevertheless, the study exposes the previously untouched problem of corneal densitometry parameters being correlated with the image background, whereas the transparency of the cornea should be adequately assessed regardless of what lies underneath it. Further work is needed to assess the effectiveness of the proposed decorrelation methods when applied to Scheimpflug images produced by other commercial devices.

In the task of finding a method for preprocessing Scheimpflug images that would decorrelate the statistical information present in the corneal ROI from that located in the image background just below that ROI (encompassing a part of anterior chamber and, in some cases, the crystalline lens and iris muscle), many normalization methods were considered. Beyond those based on the first, second, and third corneal shoulder of the one-dimensional densitometry signal (i.e., the image pixel intensity profile) that were described earlier, other features of that signal were also taken into account, such as normalization by the peak corneal value, by the root mean square value of the corneal region, and by the mean or median value of the background below corneal region, to mention just a few. Each such normalization effected the correlations between the considered densitometry parameters and the mean image background suggesting that the search for an optimal method for this task is not over. A perceived limitation of the study could be that the results are interpreted without correcting for multiple comparisons [32]. However, this correction would not affect results interpretation. Each densitometric parameter was tested for correlation against age and three biometry parameters, leading to four comparisons. In the case of the mean background, seven such comparisons were made. With Bonferroni correction that would reduce the level of significance to 0.007 whereas in all the statistically significant cases the p-values were equal to or were less than 0.005.

Modeling the statistics of corneal backscatter beyond calculating the simple mean value in each considered ROI and the utilization of the Weibull distribution deserve some comment. Unlike modeling corneal speckle in optical coherence tomography [33,34], there are no, to the best of authors knowledge, theoretical models available for such modeling in the case of corneal backscatter observed in Scheimpflug images. Therefore, any parametric (distributional) model for the corneal backscatter is essentially a trade-off between choosing the model that results in the best goodness-of-fit and adhering to the parsimony principle so that overparameterization is avoided. The two-parameter Weibull distribution has been successfully utilized to model corneal backscatter in images acquired with Corvis ST to arrive at a methodology for detecting keratoconus based on a single Scheimpflug image [35], but other models, such as gamma distribution were also successful [19]. However, the choice of a particular distributional model in the context of decorrelating its parameters from the mean image background does not appear to be an issue. When examining the nasal and temporal ROIs some asymmetry in the results have been observed. Specifically, the decorrelation of the parameter estimator $\hat{\alpha}_M$ from the mean background in the nasal region could not be achieved. The differences between nasal and temporal ROIs may stem from actual anatomical changes [36], the effect of natural UV radiation [37,38], the fact that the Scheimpflug image has an inherent geometrical distortion [39], or due to non-central position of cornea with respect to the instrument axis during acquisition. The reported image processing techniques have lead to correlations becoming in most cases insignificant but did not touch the nature of physical processes undergoing in Scheimpflug imaging. That is why those methods did not entirely resolved the problem of decoupling the biometry parameters from those of corneal backscatter.

Finally, it needs to be acknowledged that it is difficult to directly compare the results from this study to those acquired with other Scheimpflug instruments, and particularly to those that already provide estimates of corneal densitometry. Hence, the clinical efficiency of methods

Biomedical Optics EXPRESS

compensating for confounding factors in Scheimpflug-based corneal densitometry is yet to be determined.

Disclosures. Authors declare no conflicts of interest.

Data availability. Data underlying the results presented in this paper are not publicly available at this time but may be obtained from the authors upon reasonable request.

References

1. D. M. Maurice, "The structure and transparency of the cornea," The J. Physiol. **136**(2), 263–286 (1957).
2. T. Olsen, "Light scattering from the human cornea," Invest. Ophthalmol. Visual Sci. **23**(1), 81–86 (1982).
3. G. T. Smith, N. A. Brown, and G. A. Shun-Shin, "Light scatter from the central human cornea," Eye **4**(4), 584–588 (1990).
4. K. Kitagawa, Y. Sakamoto, K. Sasaki, and H. Hanaki, "Evaluation of transparency and barrier function of the cornea by Scheimpflug images," Ophthalmic Res. **28**(2), 72–77 (1996).
5. A. Wegener and H. Laser-Junga, "Photography of the anterior eye segment according to Scheimpflug's principle: options and limitations–a review," Clin. & Exp. Ophthalmol. **37**(1), 144–154 (2009).
6. M. Cherny, R. Stasiuk, P. Kelly, S. Lee, G. Golembo, and H. Taylor, "Computerised Scheimpflug densitometry as a measure of corneal opacification following excimer laser surgery," Ophthalmic Res. **26**(1), 48–54 (1994).
7. M. Koc, K. Tekin, M. I. Tekin, M. M. Uzel, P. Kosekahya, K. Ozulken, and P. Yilmazbas, "An early finding of keratoconus: increase in corneal densitometry," Cornea **37**(5), 580–586 (2018).
8. A. M. Otri, U. Fares, M. A. Al-Aqaba, and H. S. Dua, "Corneal densitometry as an indicator of corneal health," Ophthalmology **119**(3), 501–508 (2012).
9. S. N. Dhubhghaill, J. J. Rozema, S. Jongenelen, I. R. Hidalgo, N. Zakaria, and M.-J. Tassignon, "Normative values for corneal densitometry analysis by Scheimpflug optical assessment," Investig. Ophthalmol. & Vis. Sci. **55**(1), 162–168 (2014).
10. A. B. Cankaya, K. Tekin, H. Kiziltoprak, S. Karahan, and P. Yilmazbas, "Assessment of corneal backward light scattering in the healthy cornea and factors affecting corneal transparency," Jpn. J. Ophthalmol. **62**(3), 335–341 (2018).
11. T. Kampfer, A. Wegener, V. Dragomirescu, and O. Hockwin, "Improved biometry of the anterior eye segment," Ophthalmic Res. **21**(3), 239–248 (1989).
12. H. Laser, W. Berndt, M. Leyendecker, M. Kojima, O. Hockwin, and A. Cheyne, "Comparison between Topcon SL-45 and SL-45b with different correction methods for factors influencing Scheimpflug examination," Ophthalmic Res. **22**(1), 9–17 (1990).
13. A. Consejo, M. Jiménez-García, and J. J. Rozema, "Age-related corneal transparency changes evaluated with an alternative method to corneal densitometry," Cornea **40**(2), 215–222 (2021).
14. D. A. Atchison, E. L. Markwell, S. Kasthurirangan, J. M. Pope, G. Smith, and P. G. Swann, "Age-related changes in optical and biometric characteristics of emmetropic eyes," J. Vis. **8**(4), 29 (2008).
15. B. Winn, D. Whitaker, D. B. Elliott, and N. J. Phillips, "Factors affecting light-adapted pupil size in normal human subjects," Invest. Ophthalmol. Visual Sci. **35**(3), 1132–1137 (1994).
16. A. Prasad, K. Fry, and P. S. Hersh, "Relationship of age and refraction to central corneal thickness," Cornea **30**(5), 553–555 (2011).
17. R. A. Armstrong, "Statistical guidelines for the analysis of data obtained from one or both eyes," Ophthalmic Physiol. Opt. **33**(1), 7–14 (2013).
18. D. Szczesna and H. Kasprzak, "The modelling of the influence of a corneal geometry on the pupil image of the human eye," Optik **117**(7), 341–347 (2006).
19. A. Consejo, K. Gławdecka, K. Karnowski, J. Solarski, J. J. Rozema, M. Wojtkowski, and D. R. Iskander, "Corneal properties of keratoconus based on Scheimpflug light intensity distribution," Investig. Ophthalmol. & Vis. Sci. **60**(8), 3197–3203 (2019).
20. R. Faragher, B. Mulholland, S. Tuft, S. Sandeman, and P. Khaw, "Aging and the cornea," Br. J. Ophthalmol. **81**(10), 814–817 (1997).
21. B. Lopes, I. Ramos, and R. Ambrósio Jr, "Corneal densitometry in keratoconus," Cornea **33**(12), 1282–1286 (2014).
22. M. Pakbin, M. Khabazkhoob, M. Pakravan, A. Fotouhi, E. Jafarzadehpur, M. Aghamirsalim, and H. Hashemi, "Corneal Scheimpflug densitometry in photorefractive keratectomy candidates," Cornea **39**(11), 1381–1388 (2020).
23. G. Cennamo, R. Forte, B. Aufiero, and A. La Rana, "Computerized Scheimpflug densitometry as a measure of corneal optical density after excimer laser refractive surgery in myopic eyes," J. Cataract. & Refract. Surg. **37**(8), 1502–1506 (2011).
24. M. Alnawaiseh, L. Zumhagen, S. Zumhagen, L. Schulte, A. Rosentreter, F. Schubert, N. Eter, and G. Mönnig, "Corneal densitometry as a novel technique for monitoring amiodarone therapy," Ophthalmology **123**(11), 2294–2299 (2016).
25. X. Yang, Q. Liu, Q. Feng, and H. Lin, "Safety and efficacy of corneal minimized-volume ablation with accelerated cross-linking in improving visual function for keratoconus," Cornea **39**(12), 1485–1492 (2020).

Biomedical Optics EXPRESS

26. M.-R. Sedaghat, H. Momeni-Moghaddam, J. Heravian, M. W. Belin, R. Ambrósio Jr, T. Gheysari-Alishahi, and S. H. Ghavami, "Scheimpflug corneal densitometry changes after the intrastromal corneal ring segment implantation," Cornea **39**(6), 761–768 (2020).
27. R. L. Niederer, D. Perumal, T. Sherwin, and C. N. J. McGhee, "Age-related differences in the normal human cornea: a laser scanning in vivo confocal microscopy study," Br. J. Ophthalmol. **91**(9), 1165–1169 (2007).
28. A. Daxer, K. Misof, B. Grabner, A. Ettl, and P. Fratzl, "Collagen fibrils in the human corneal stroma: structure and aging," Invest. Ophthalmol. Visual Sci. **39**(3), 644–648 (1998).
29. S. Sharma, V. Tobin, P. R. J. Vas, R. A. Malik, and G. Rayman, "The influence of age, anthropometric and metabolic variables on ldiflare and corneal confocal microscopy in healthy individuals," PLoS One **13**(3), e0193452 (2018).
30. D. A. Jesus and D. R. Iskander, "Assessment of corneal properties based on statistical modeling of OCT speckle," Biomed. Opt. Express **8**(1), 162–176 (2017).
31. T. Hillenaar, R. H. H. Cals, P. H. C. Eilers, R. J. Wubbels, H. van Cleynenbreugel, and L. Remeijer, "Normative database for corneal backscatter analysis by in vivo confocal microscopy," Investig. Ophthalmol. & Vis. Sci. **52**(10), 7274–7281 (2011).
32. R. A. Armstrong, "When to use the bonferroni correction," Ophthalmic Physiol. Opt. **34**(5), 502–508 (2014).
33. R. G. Gary, J. P. Rolland, and K. J. Parker, "Speckle statistics of biological tissues in optical coherence tomography," Biomed. Opt. Express **12**(7), 4179–4191 (2021).
34. M. Niemczyk and D. R. Iskander, "Statistical analysis of corneal OCT speckle: a non-parametric approach," Biomed. Opt. Express **12**(10), 6407–6421 (2021).
35. A. Consejo, J. Solarski, K. Karnowski, J. J. Rozema, M. Wojtkowski, and D. R. Iskander, "Keratoconus detection based on a single Scheimpflug image," Transl. Vis. Sci. & Technol. **9**(7), 36 (2020).
36. M. Koç, K. Özülken, O. Ayar, and A. Karakurt, "Measurement of the anterior chamber angle according to quadrants and age groups using Pentacam Scheimpflug camera," J. Glaucoma **22**(3), 226–229 (2013).
37. D. H. Sliney, "How light reaches the eye and its components," Int. J. Toxicol. **21**(6), 501–509 (2002).
38. P. E. King-Smith, T. F. Mauger, C. G. Begley, and P. Tankam, "Optical analysis and reappraisal of the peripheral light focusing theory of nasal pterygia formation," Investig. Ophthalmol. & Vis. Sci. **61**(2), 42 (2020).
39. M. Dubbelman, V. Sicam, and G. Van der Heijde, "The shape of the anterior and posterior surface of the aging human cornea," Vision Res. **46**(6-7), 993–1001 (2006).